ELSEVIER

Catalysis Today 41 (1998) 409–432

CATALYSIS TODAY

Selective gas-phase oxidation at oxide nanoparticles on microporous materials

Jin S. Yoo[1]

Samsung Chemical Group, Samsung Corporation, Seoul, South Korea

Abstract

Catalytic oxidation over single metal or bimetallic oxides in nano-size generated on various matrices including zeolite via the chemical vapor deposition (CVD) technique and other methods are reviewed along with other interesting catalytic reactions. Among the various matrices studied, the partially deboronated borosilicate (DBH) played a unique role for the para-selective oxidation of alkylaromatics. The CVD Fe/Mo/DBH activated by the proper calcination procedure exhibited higher catalytic activity, better product selectivity, and superior stability to form aldehydes, in particular, terephthaldehyde and *p*-tolualdehyde, by the gas-phase O_2 oxidation of *p*-xylene than its impregnated counterpart and bulk catalytic material. Current mechanistic understanding on the unusual promoting role of CO_2 over the same catalyst was postulated for the O_2 oxidation reaction.

The silica overlayer in nano-size deposited on zeolite by the CVD of silicon alkoxides not only increased the para-selective property, but also provided other useful functions such as control of pore opening and thermal stability of the zeolite catalyst. Other oxidation reactions such as oxidative dehydrogenation of alkylaromatics and alkanes were also reviewed along with the selective N_2O oxidation of benzene to phenol.

CVD Fe/Mo/ZSM-5 oxidized *p*-xylene to produce aldehydes, but disproportionation and dehydrocoupling of *p*-xylene to toluene and pseudocuemen, and trimethylbiphenyl-methane, respectively, remained the predominant reactions.

Keywords: Oxide nanoparticle; CVD Fe/Mo/DBH; Gas-phase O_2 oxidation; Alkylaromatics

1. Introduction

Nanocrystalline materials are solid-state systems constituting of crystallites 5–20 nm in dimension. Various techniques have been adopted for their syntheses [1,2]. Gas-phase synthesis [3], chemical vapor deposition (CVD) [4–6], metal oxide vapor synthesis [7,8], CVD and decomposition [9], sonochemical decomposition [10–12], the rapid thermal decomposition of precursors in solution method [13], hydrodynamic cavitation [14], preparation in flame [15], the sol–gel process [16–18], in particular, a complexing agent assisted sol–gel method [19], gel-supported precipitation [20], and aerosol processes including evaporative decomposition of solutions, spray pyrolysis [21], high temperature aerosol decomposition, mist decomposition, aerosol thermolysis, aerosol high temperature decomposition [22], and a combina-

[1]Present address: 2315 Mast Court, Flossmoor, IL 60422, USA. Tel.: 001-708 798-4998; fax: 001-708 798-2533; e-mail: jsyoo@worldnet.att.net.

0920-5861/98/$32.00
PII S0920-5861(98)00028-5

tion of sol–gel method and impregnation technique [23] have been known for preparation of nano-size particles.

Among these methods, the laser-induced CVD and photochemical vapor depositions of a variety of metals, Ga, In, Sb, Au, W, Al, and Te, and metalloids such as As, P, and Si have been extensively utilized in the semiconductor and solar cell industry. In particular, the CVD of silica film using $Si(OR)_4$ becomes a key process in producing semiconductor devices [24–28].

Extensive efforts are also being made to develop H_2, O_2, CO, N_2, H_2S, and CO_2 permselective microporous inorganic membranes by applying the same CVD technique. In general, silane derivatives are used for a thin layer of silica deposition, and the sol–gel method is also used to coat a thin silica film on top of the substrate materials.

The CVD technique has attracted an unusual attention from the catalyst manufacturing industry. The technique has been employed for uniformly depositing the well dispersed fine particles of nano-size of the catalytic materials such as metal and metal oxide on a supporting matrix. These CVD catalysts tend to exhibit higher catalytic stability, better and novel catalytic performance differing from their counterparts prepared by the conventional techniques [29,30]. The technology was also applied to modify the catalyst surface structure with the silica layer [31,32], and the V_2O_5 thin film [33].

In this paper, CVD single metal or bimetallic oxides/zeolite or other supporting matrices, which are active for the oxidation reaction, are reviewed along with the modification of zeolites by the CVD silica film. Focus was on the catalytic behaviors of single metal or bimetallic oxide catalysts deposited on various zeolite matrices or other supports. In particular, among bimetallic oxide catalysts prepared by the CVD technique, CVD M/M′/DBH catalysts, where M and M′ stand for Fe(III), Zn(II), Zr(IV), Nb(V), In(III), Sn(IV), Sb(V), Ce(IV), Bi(III), and Mo(VI), W(VI), V(V), respectively, the CVD Fe/Mo/DBH catalyst was found to be the most active and selective for the synthesis of terephthaldehyde and *p*-tolualdehyde from the gas-phase O_2 oxidation of *p*-xylene in the fixed bed quartz reactor [34].

The CVD Fe/Mo/DBH molecular sieve prepared by the CVD technique, its silica-coated system, SiO_2/Fe/Mo/DBH, and the impregnated counterpart prepared by the conventional incipient wetness method are studied for the gas-phase O_2 oxidation of alkylaromatics to the corresponding aldehydes and other oxygenates. The CVD Fe/Mo/DBH catalyst was thoroughly characterized by Raman spectroscopy and electron microscopy, and proved that the active catalytic species, $Fe_2(MoO_4)_3$, were uniformly dispersed as nanoparticles (2–40 nm) on the surface. This is reflected on the superior catalyst performance and better stability over its impregnated counterpart for the para-selective gas-phase O_2 oxidation of methylaromatiacs to the corresponding aldehydes in a high selectivity.

A series of para-selective oxidation of alkylaromatics, *p*-substituted toluene derivatives, oxidative dehydrogenation of alkylaromatics and alkanes, selective hydroxylation of benzene to phenol with N_2O over the catalysts prepared by CVD, gel coformation, and aerogel methods was also briefly reviewed along with other interesting catalyses, which are unique to the nano-structured materials.

2. Experimental

2.1. *Preparation of CVD* Fe/Mo*/DBH*

The surface silanols on the borosilicate molecular sieve were used as anchoring sites for metallic component in the preparation of the catalyst. The partially deboronated borosilicate (DBH) having an MFI structure containing 0.25 and 0.013 wt% boron have been determined to have 10 and 20 wt% silanol groups, respectively, by ^{29}Si magic angle spinning nuclear magnetic resonance. The partially boronated borosilicate (DBH) based catalyst was prepared by the CVD technique from $FeCl_3$ or MoO_2Cl_2 $MoOCl_4$, and $MoCl_5$. The preparation procedure was reported in detail elsewhere [4]. Other types of nano-size catalysts such as single metal and bimetallic oxides on various types of zeolites and other matrices were also prepared by CVD, gel coformation, and aerogel technique, and the pertinent references describing details of these procedures were cited for each catalyst.

2.2. *Characterization of CVD* Fe/Mo*/DBH*

The CVD Fe/Mo/DBH catalyst was thoroughly characterized by employing combined high resolution electron microscopy (HREM), temperature programmed oxidation (TPO) and temperature programmed reduction (TPR), NH_3 desorption, X-ray powder diffraction, X-ray photoelectron spectroscopy, and in situ total electron yield near edge spectroscopy (XANES) [35]. Two phases, $Fe_2(MoO_4)_3$ and MoO_3, were identified by Raman spectroscopy and XRD methods, and it was confirmed that $Fe_2(MoO_4)_3$ was an active species for the para-selective oxidation of alkylaromatics to aldehydes in the gas-phase O_2 oxidations.

The typical microstructures of two CVD Fe/Mo/DBH samples are shown in Fig. 1 ((a) fresh sample as received, and (b) the counterpart calcined in air for a prolonged period). At low magnifications, the molecular sieve particles in the fresh sample appear to have a rather uniform contrast. Only at higher magnifications, very small dark particles begin to appear. The energy dispersive X-ray emission study (EDXS) analyses indicated that Fe and Mo are finely dispersed inside the main channel of the DBH matrix. In addition, Fe and Mo are always associated with each other. In the calcined counterpart in Fig. 1(b), very small dark particles are apparent at lower magnifications, which have the compositions similar to either $Fe_2(MoO_4)_3$ or $FeMoO_4$, as identified by EDXS analyses.

HREM of fresh CVD Fe/Mo/DBH clearly show that most Fe/Mo-rich domains (with a darker contrast) have a rod-like shape with diameters ranging from 1 to 10 nm. More significantly, these rod-like Fe/Mo-rich domains tend to be oriented along the two micropore channel systems as defined by the DBH framework. Fig. 2 shows the JREM micrograph of an area from the calcined CVD Fe/Mo/DBH counterpart, which shows that the previous rod-like particles have rearranged into nearly spherical Fe/Mo rich particles. These particles are dispersed on the DBH with sizes ranging from 20 to 40 nm. Occasionally, larger Fe/Mo particles (greater than 50 nm in size) are observed, which are located exterior to the DBH particle. As indicated before, the Fe/Mo-rich particles are either $Fe_2(MoO_4)_3$ or $FeMoO_4$. The HREM observation provides clear insight into the pathway for the deposition of Fe and Mo during CVD, that is, via the two

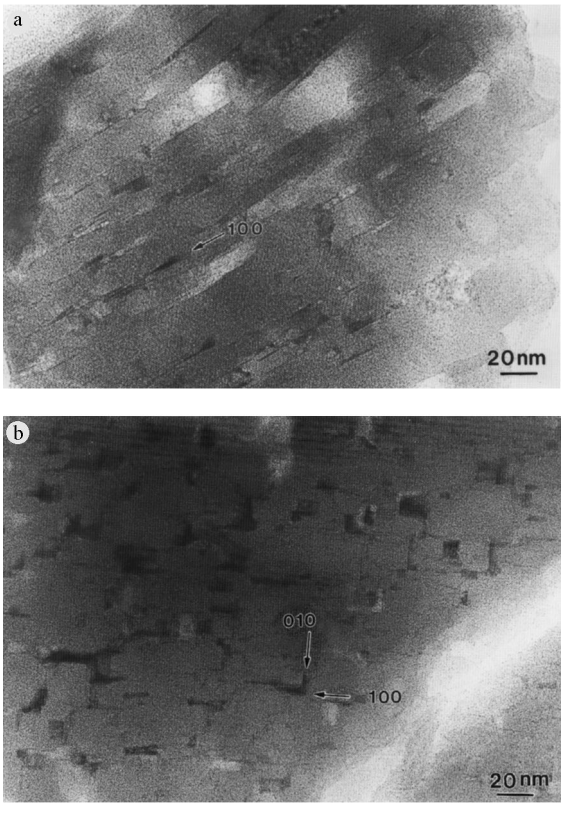

Fig. 1. High resolution electron micrographs of CVD Fe/Mo/DBh: (a) fresh; (b) calcined at 650°C for a prolonged period.

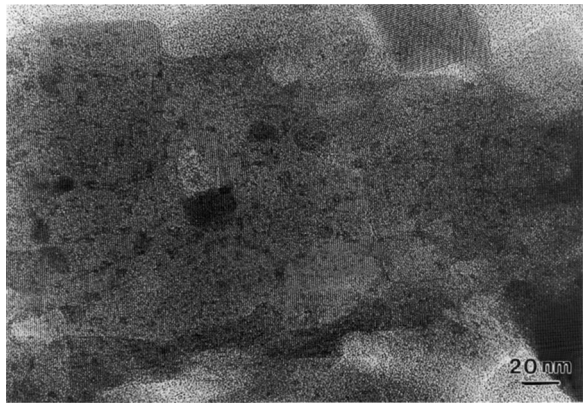

Fig. 2. High resolution electron micrographs showing lattice image of DBH molecular sieve with ''darker'' ferric molybdate regions.

primary micropore channel system. This pathway of Fe/Mo deposition has a predominant effect in confining the Fe/Mo into the DBH in the final catalyst. Although the shape and size of the $Fe_2(MoO_4)_3$/$FeMoO_4$ particles have changed due to significant Fe and Mo migrations, the majority of the particles are dispersed within the DBH molecular sieve [35].

The processes of CVD deposition and calcination appear to introduce minor and localized destruction of the DBH crystalline structure, as shown in Figs. 1 and 2. However, the density of such localized defect regions is so small that macroscopically speaking, both fresh and calcined molecular sieves have nearly perfect crystalline structure. It is also interesting to note that the prolonged calcination process seems to have some healing effect on these localized defect regions, as suggested by the apparent overall lower density of defect regions in the calcined CVD Fe/Mo/DBH. The activated catalyst by prolonged calcination performed much better than the fresh counterpart for the oxidation of *p*-xylene.

In situ low temperature CO_2-dosing XANES experiments provided an evidence for a strongly chemisorbed CO_2 species on the Fe-site of the CVD Fe/Mo/DBH catalyst at the reaction temperature [35]. This may have some bearings on the dramatic effect of CO_2 observed in the oxidation of *p*-xylene and other alkylaromatics over the catalyst.

2.3. *Evaluation of catalytic activity of CVD* Fe/Mo*/DBH and product analysis*

Evaluation of the catalyst and product analysis were carried out according to the procedures described elsewhere [4].

3. Results and discussion

3.1. *Modification of zeolite by CVD* SiO_2

Many efforts are currently being made to modify and design new speciality materials including zeolite and other types of catalytic materials by various research groups throughout the world [9]. Some of the efforts have already been commercialized to provide a big impact on the industry. Numerous other works are showing promising signs for potential applications in many fields such as specialty chemical syntheses, permselective membrane, ceramic materials, semiconductor, new electronics, photovoltaic cell, and so forth.

3.1.1. *CVD silica film*

Zeolites have been modified by depositing a catalytic moiety on the exterior and/or within the interior structure for pore-size engineering [36], modification of the properties, and preparation of bifunctional catalysts by depositing a catalytic material. Attempts have been made and are still being made to control the pore size by coating a SiO_2 layer on the external surface of zeolites. At the same time, acidity of the zeolite can also be manipulated by the same procedure. Silicone alkoxides are usually deposited on the exterior surface, while with silane, SiH_4, the interior pores are also coated due to the smaller molecular size of silane as well as the external surface [37].

The external pore size opening of a H-mordenite was reduced by 0.1 and 0.2 nm, depending on the number of silica layer formed (1 to 2 and 3 layers, respectively) by depositing $Si(OCH_3)_4$ [38]. The CVD reaction occurs initially on the external surface according to the following scheme. The deposited species are converted to a silica layer by calcining at 400°C.

$$x\text{Z-OH} + \text{Si(OCH}_3)_4 \rightarrow (\text{Z} - \text{O})_x\text{Si(OCH}_3)_{4-x} + x\text{CH}_3\text{OH}$$

3.1.2. *Catalytic reactions processes*

Alkylation, isomerization and disproportionation. Alkylation of toluene with methanol and toluene disproportionation to make *p*-xylene have been carried out over HZSM-5 modified with CVD silicon alkoxide (Si/HZSM-5) [39,40]. As the silica deposition amount increased, the selectivity to *p*-xylene in the xylene product increased to more than 98%. Fig. 3 shows the change in the xylene isomer yield when alkylation of toluene with methanol was carried out with CVD Si/ZSM-5 [40]. Over the untreated ZSM-5, the ratio of *o*-, *m*-, and *p*-xylene isomers is approximately 1:2:1, which agrees with the thermodynamic values. On the other hand, with the silica treated counterpart, the formation of *o*-and *m*-xylene having somewhat larger molecular size was suppressed, and conse-

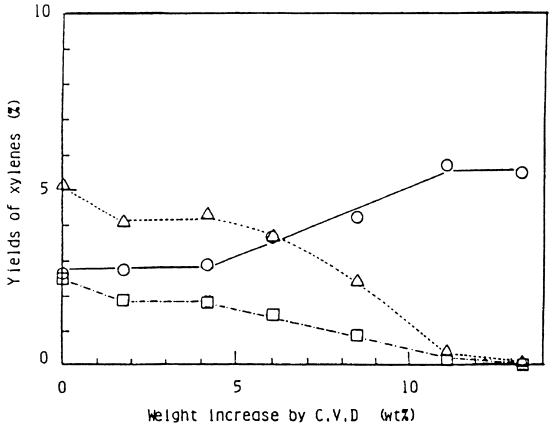

Fig. 3. Shape selectivity generated on the silica deposited ZSM-5 in alkylation of toluene with methanol: *o*- (□), *m*- (△) and *p*-xylene (○).

quently, *p*-xylene formation increased. Such a remarkable change in the product distribution was also observed in both isomerization of xylene and disproportionation of toluene. This shape selectivity is attributable to strict control of the pore size by the CVD SiO_2 deposition.

Disproportionation of ethylbenzene to p-diethylbenzene. A commercial *p*-diethylbenzene process was recently developed using disproportionation of ethylbenzene, and alkylation reaction of benzene with ethanol by depositing SiO_2 on the MFI zeolites [41].

The results for disproportionation of ethylbenzene are summarized in Table 1. A pilot plant having 100 t/y capacity has been operated in India since 1993, and the selectivity of *p*-isomer in the disproportionated product, *p*-diethylbenzene, reaches 100% with the silica treated MFI zeolite containing 16 wt% SiO_2. Even if the conversion level is decreased to about one-half, the conversion level can be maintained by increasing the contact time in this process.

Table 1
Disproportionation of ethylbenzene over SiO_2/MFI zeolite

Catalyst	SiO_2-treated MFI zeolite	Untreated MFI zeolite
WHSV/h	2.9	5.8
Conv. (%) of ethylbenzene (%)	12.5	12.83
Select to diethylbenene (%)	54.72	56.66
Para-isomer	99.42	33.43
Meta-isomer	0.53	63.96
Ortho-isomer	—	2.61

Temperature: 300°C, H_2/HC=2/1.

Selective hydrogenation of terminal double bond in olefins. Methoxytripropylsilane was found to be effective to make the CVD SiO_2/HZSM-5 for controlling pore opening of the exterior surface [40]. It has been a difficult task to selectively hydrogenate the terminal double bond over the internal double bond or vice versa with the solid catalyst. When Pt-ion exchanged zeolite 4A was CVD treated with $Si(OEt)_4$, the terminal double bond was preferentially hydrogenated over the internal one [42,43].

Selelctive lactam synthesis. Sato et al. discovered that the neutral silanol group on the exterior surface was responsible for the conversion of oxime (100%) and selectivity toward lactam (95%) in the gas-phase Beckmann rearrangement [44,45].

Alkane cracking. The cracking reaction of octane and 2,2,4-trimethylpentane (TMP) over the silica coated mordenite (SiHM) is shown in Fig. 4. HM was active for cracking both octane and TMP, but an extremely high shape selective property was exhibited by SiHM [46].

Rearrangement of m-dioxane. *m*-Dioxane could be rearranged to neo-alkylaldehydes at 250–400°C by enhancing the catalytic activity of various zeolites such as HZSM-5, USY and pentasil via CVD deposition of Si alkoxides [47].

3.1.3. *Catalyst selectivity improvement by an inactivation process*

Inumaru et al. proved experimentally that the activity of vanadium phosphate catalyst differed from the crystalline face by using an idea that made the catalyst inactive by covering the catalyst surface with a silica film [48]. After the catalyst was completely covered initially with the CVD silica film, and then the crystal was destroyed to expose a certain crystalline face, the catalytic activity appeared.

In order to suppress the photocatalytic decomposition of perfume in the cosmetics by a pigment, TiO_2, on exposure to the UV light, a commercial process for the treatment of TiO_2 with 1,3,5,7-tetramethylcyclotetrasiloxane by the CVD technique has been developed based on this principle [49].

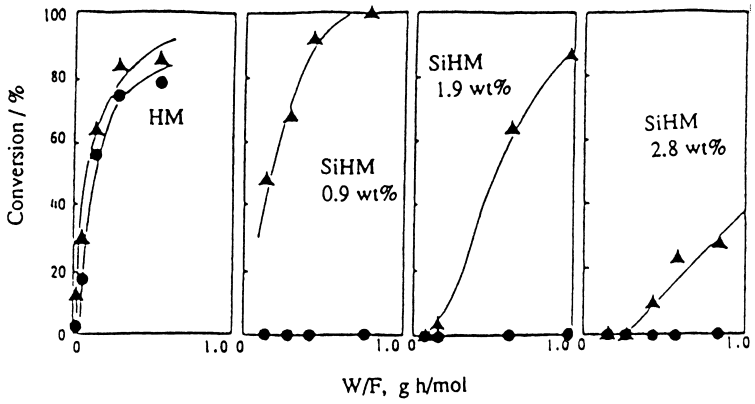

Fig. 4. Cracking reactions for octane (▲) and 2,2,4-TMP (●) on HM and SiHM at 300°C; size: octant (0.43 nm) and 2,2,4-TMP (0.62 nm).

3.1.4. *New* SnO_2*-based molecular sieve*

The SnO_2-based molecular sieve was prepared by using a unique method: an organic template such as benzaldehyde was adsorbed to the extent that approximately one-half of the SnO_2 surface could be covered, and the rest was covered with silica. By removing the template with NH_3 as benzonitrile, a silica layer having a hole of a benzene ring size was prepared on the SnO_2 [50]. This should function as a molecular sieve.

The procedure for the preparation of SnO_2-based molecular sieve, silica overlayer on SnO_2 using an organic template molecule, is illustrated above.

3.2. *CVD single metal oxide on zeolite*

Ti-*silicalite*. The nature of active titanium species for epoxidation of olefins with H_2O_2 and tert-butylhydroperoxide for titania deposited on a silica support via CVD was studied by Ito et al. [51] and the results

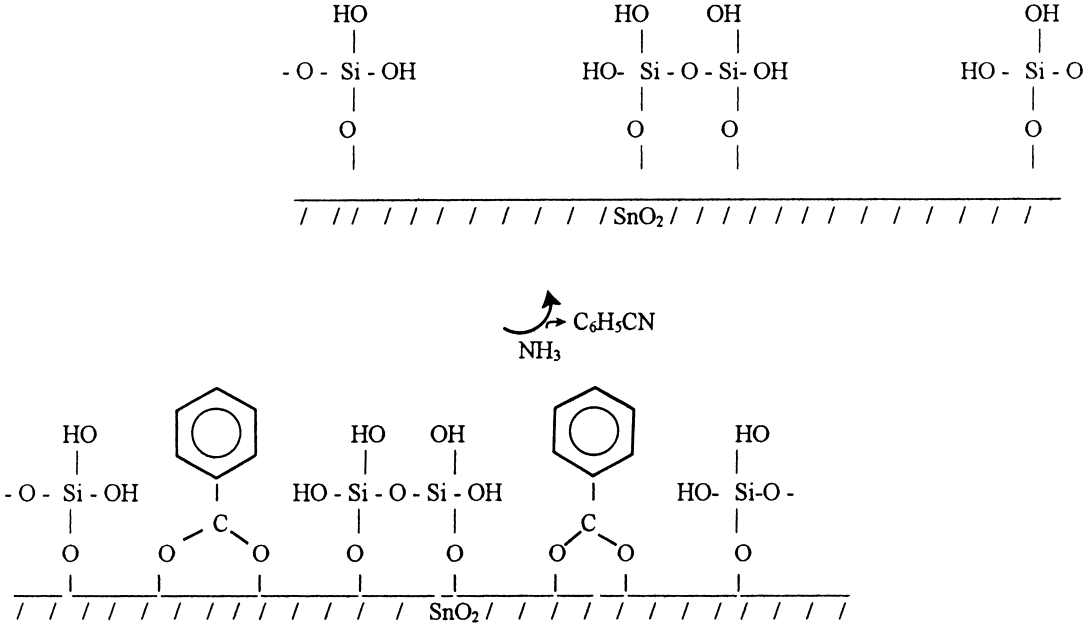

were compared with Ti–silicalite (TS-1) and titania–silica prepared by sol–gel methods. IR and XANES analyses suggested that in titania–silica and in the CVD catalyst has a tetrahedral configuration bonded to SiO_2 and that Ti in TS-1 has a configuration composed of >Ti–O or related to it. These configurations are closely related to the catalytic activities in olefin epoxidation; the former works with tert-butyl hydroperoxide and the latter with H_2O_2.

Pt/*KL zeolite*. Platinum hexafluoroacetylacetonate was selectively introduced inside the channels of KL zeolite (Linde type L) via CVD in a flow of Ar at 170°C. Small non-acidic Pt clusters of nucleophilic nature were formed. The catalyst showed remarkably high activity and selectivity for the conversion of methylcyclopentane to benzene at 500°C [52,53].

Ga/*HZSM-5*. Ga/HZSM-5 was prepared using $GaCl_3$ and HZSM-5 by the CVD method [54]. As more protons are being substituted by $(GaO)^+$, the conversion of propene to aromatics decreases, but that of propane passes through a maximum, and so does the aromatics selectivity. This is consistent with a bifunctional mechanism in which Brønsted acid sites catalyze oligomerization and ring closure, but Ga, in concert with protons, acts as a dehydrogenation site.

$Mo(CO)_6$/*X-, Y-zeolite*. Okamoto et al. [55,56] investigated the behavior of $Mo(CO)_6$ supported inside the X- and Y-zeolite cages by EXAFS, XPS, and IR, and observed that the Mo–Mo bond was not observed but newly formed Mo–O bond was observed. They also reported the formation of fac-$Mo(CO)_3(OZ)_3$ (OZ stands for zeolite lattice oxygen). The resulting partially decarbonylated species are an excellent catalyst for the selective hydrogenation of butandiene and pentadiene to the corresponding *cis*-olefins. It has also been known that the partially decarbonylated metal subcarbonyls, $M(CO)_x$ (x=3,4,5), in particular, $M(CO)_3$ is an active species for metathesis, but the $M(CO)_2O_2$ species resulting from O_2 adsorption showed 15 times the original activity of $M(CO)_3$ [57].

Pd/Na*Y or* Na*HY zeolite*. Coke was deposited on the acidic sites of the reforming catalyst, and it became the main cause for the catalyst deactivation. Pd ion exchanged zeolite was usually produced using $[Pd(NH_3)_4]^{2+}$, and H^+ was stoichiometrically produced upon H_2 reduction according to the following reaction:

$$Pd^{2+} + H_2 \rightarrow 1/n[Pd^0]_n + 2H^+$$

The H^+ produced in this manner should be removed from the system by an ion exchange with Na^+. Non-acidic Pd/zeolite catalyst was prepared in a single step by fixing an organic Pd-complex having an appropriate molecular size inside the zeolite cage [58]. The Pd particles having nano-size were produced by removing the organic complex via reduction reaction with H_2 according to the following equation:

$$PdL_x/\text{zeolite} + x/2\,H_2 \rightarrow 1/n[Pd^0]_n + xLH$$

NaY or NaHY were placed in the middle portion of a U-tube with quartz wool, and treated at 25–400°C. Then, a precursor such as $[Pd(\eta^3\text{-}C_3H_5)(\eta^5\text{-}C_5H_5]$ placed at the bottom of the U-tube was sublimated in Ar (10 ml/min) at 25°C [59] followed by the H_2 reduction to prepare the CVD Pd/zeolite catalyst. The resulting catalyst exhibited 100% selectivity for the ring opening hydrogenation reaction of methylcyclopentane.

$Fe_3(CO)_{12}/SiO_2$. When $Fe_3(CO)_{12}$ was supported on silica by CVD, a new $Fe_3(CO)_6$ cluster, which could not be found in the solution, was formed [60]. According to the EXAFS analysis, the Fe–Fe distance (0.273 nm) in $Fe_3(CO)_6$ is longer than that of $Fe_3(CO)_{12}$ (0.262 nm) and that of the metal (0.248 nm). The resulting cluster catalyst was active for hydrogenation of propene, and its catalytic activity showed 200 times that of the SiO_2 supported $Fe_3(CO)_{12}$ prepared by the impregnation method. It indicates that the coordinatively unsaturated sites and the Fe–Fe bond character remarkably affect the catalytic activity.

V_2O_5/TiO_2. The CVD V_2O_5/TiO_2 catalyst was prepared from $VOCl_3$ and surface OH-group on TiO_2, and the resulting catalyst was excellent for the selective oxidation of *o*-xylene to phthalic anhydride, and exhibited much superior activity to the impregnated counterpart [61,62]. The same catalyst displayed quite different TOF over the conventionally prepared impregnation counterpart for oxidation of H_2, ammonia and benzene. It is surmised that the property of the surface V=O bond must be different in these two catalysts [63].

Mo/SiO2. The Mo/SiO_2 catalyst was prepared by heating MoO_3 onto the SiO_2 matrix by the metal oxide vapor synthesis (MOVS) technique [7]. This catalyst exhibited high activity for the oxidation of methanol to formaldehyde [7,8].

CVD Sn/SiO_2. The Sn supported silica catalyst was prepared according to the procedure reported in [64]. The resulting CVD catalyst displayed higher catalytic activity and selectivity for oxidative dehydrogenation of ethylbenzene than the impregnation counterpart. A cause for the better catalytic performance is attributed to well dispersed SnO_2 microparticles having an appropriate acidity.

As mentioned above, bimetallic oxides in nano-size were deposited on zeolite matrices by the CVD technique. Over the resulting catalysts, the gas-phase O_2 oxidation of methylaromatics and to aldehydes and alkenylaromatics, respectively, and N_2O oxidation of benzene to phenol were studied, and the results were reviewed.

3.3. *Oxidation of p-xylene over CVD* Fe/Mo*/DBH*

The CVD Fe/Mo/DBH was prepared from $FeCl_3$, MoO_2Cl_2 (or $MoCl_5$, $MoOCl_4$) and borosilicate molecular sieve, HAMS-1B-3, by the CVD procedure described elsewhere [4]. The fresh CVD Fe/Mo/DBH catalyst was calcined in air for one day at 680°C. The atomic ratio of Mo/Fe in the fresh catalyst was altered from the initial 3.3/1 to 1.8/1 during the calcination period, and this indicates that the excess Mo over the stoichiometry (Mo/Fe=1.5) of $Fe_2(MoO_4)_3$ sublimed off and condensed as white MoO_3 needle crystals on the cooler part of the reactor.

Ultimately the Mo/Fe ratio approaches the stoichiometry of $Fe_2(MoO_4)_3$ in the prolonged air calcination process. Raman spectra of the calcined catalyst and its precursor are shown in Fig. 5. The resulting fresh and calcined catalysts were subjected to the gas-phase O_2 oxidation of *p*-xylene at 375°C in the microreactor [4]. The results are compared in Table 2.

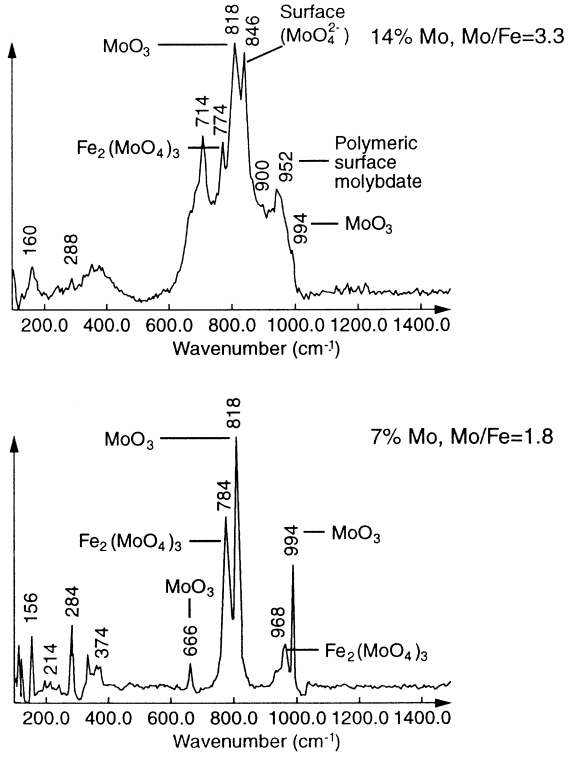

Fig. 5. Raman spectra of fresh CVD Fe/Mo/DBH and activated catalyst calcined for a prolonged period.

Table 2

Catalyst	O_2/*p*-Xylene	*p*-Xy-Product selectivity (%)				
		Conv.	TPAL	TOAL	CO_2	Byprod.
Fresh	10	20	39	18	37	6
Calcn.	10	68	47	21	19	13

3.3.1. *CVD catalyst versus impregnated catalyst*

The impregnated counterpart of the CVD Fe/Mo/DBH was prepared with $Fe(NO_3)_3$ and ammonium polymolybdate onto borosilicate molecular sieve,

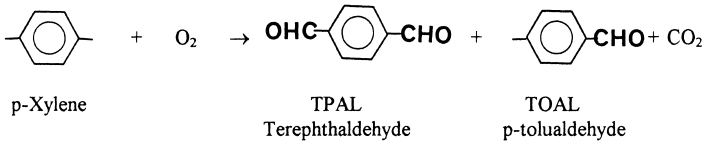

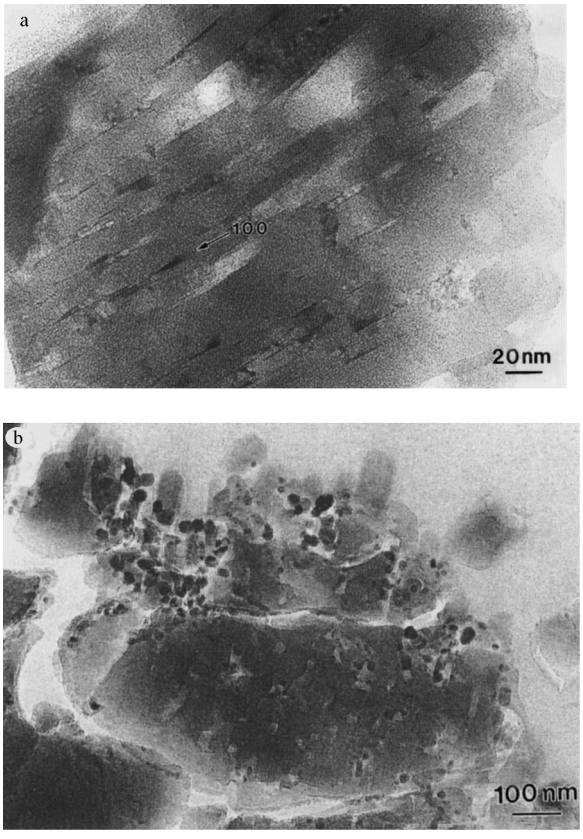

Fig. 6. TEM (a) CVD Fe/Mo/DBH versus (b) impregnated Fe/Mo/DBH.

HAMS-1B-3, by the conventional incipient wetness technique. It was activated by calcination in air at 650°C for a prolonged period. The electron micrograph of the resulting catalyst is shown in Fig. 6. It is quite in contrast to that of the CVD counterpart. Aggregates of the metal moieties constituting both MoO_3 and $Fe_2(MoO_4)_3$ are dispersed heterogeneously mostly on the exterior surface. The resulting impregnation catalyst and its CVD counterpart were evaluated for the gas-phase O_2 oxidation of *p*-xylene under comparable reaction conditions, and compared the results in Table 3. The results show that the CVD catalyst is far superior to its impregnated counterpart in the catalyst performance. The catalyst aging tests were also carried out with these catalysts in the regular quartz reactor for a long period. The results also lead to conclude that the CVD catalyst is much more stable over its impregnated catalyst [65]. A significant amount of the catalyst species was leached out of the impregnated catalyst while its CVD counterpart did not show any sign of deactivation. Much higher temperatures were required to get the same *p*-xylene conversion over the bulk $Fe_2(MoO_4)_3$ than the CVD counterpart.

3.3.2. *Para-selective oxidation*

With the CVD Fe/Mo/DBH catalyst, *ortho*- and *meta*-xylene were separately evaluated in a microreactor at 350–400°C, and the results are compared with that of *p*-xylene in Table 4. It leads to the

Table 3
Evaluation of catalyst performances, impregnation versus CVD technique

	Temp. (°C)					
	235	350		375	400	
	CVD	Impr.	CVD	Impr.	CVD	Impr.
p-Xylene conv. (%)	(43.3)[a]	21.4	(74.7)	32.6 [69.2]	(96.7)	61.6
Product selectivity (%)						
TPAL	(48.3)	18.7	(39.4)	3.5 [4.1]	(23.3)	18.1
TOAL	(33.7)	46.4	(24.9)	42.6 [48.6]	(24.9)	44.7
Benzaldehyde	(2.0)	0.8	(2.5)	1.0 [0.9]	(25.0)	1.0
MA[b]	(5.7)	0.2	(9.8)	0.0 [0.0]	(17.0)	0.9
CO	(2.7)	5.9	(5.3)	8.1 [6.9]	(11.1)	7.6
CO_2	(6.6)	26.1	(14.0)	32.3 [33.5]	(28.2)	25.4

[ ]: With 2% steam.
[a]Run conditions: contact time, 0.21 s; WHSV, 0.23 h; premixed gas: 0.1% *p*-xylene, 1.0% O_2, and 1.0% N_2 in He.
[b]Maleic anhydride.

Table 4
Reactivity of xylene isomers over CVD Fe/Mo/DBH

	Xylene isomer						
	o-Xylene		*m*-Xylene		*p*-Xylene		
Temp. (°C)	350	400	350	400	350	325[a]	350[a]
Conversion (%)	6	14	3	9	78	32	58
Product selectivity (%)							
Monoaldehyde	33	14	67	33	0	26	22
Dialdehyde	Trace	Trace	0	0	44	55	48
PTAN		29					
TMBPM	0	21					
MA	0	0	0	0	12	0	0
CO		29				4	
CO_2	66		33	67	18		

Reaction conditions: O_2/xylene: 43/1, contact time: 0.15 s, WHSV: 0.32 h^{-1}.
[a]O_2:xylene=10/1, PTAN: phthalic anhydride, MA: maleic anhydride, TMBPM: trimethylbiphenylmethane.

conclusion that the reactivity of xylene isomers on the catalyst is in the order *p*-xylene≫*o*-xylene>*m*-xylene. In other words, the CVD Fe/Mo/DBH catalyst exhibits a para-selective property for the oxidation of xylene isomers. This large reactivity difference observed with the xylene isomers may be attributed to the difference in the molecular geometry of xylene isomers and the unique surface structure of the catalyst. Together with these factors, it may be explained by the two types of active sites postulated based on chemical modeling work elsewhere [66].

3.3.3. *Separation of p-xylene from xylene isomers mixture containing ethylbenzene*

Attempts were made to prove the validity of the concept that *p*-xylene can be selectively separated from its xylene mixture by taking advantage of the big reactivity gap existing between *p*-xylene and *o*-/*m*-xylene over CVD Fe/Mo/DBH for the gas-phase O_2 oxidation of xylene isomers. The xylene mixture containing the thermodynamic equilibrium composition of *p*-xylene:*m*-xylene:*o*-xylene=1:2:1 was subjected to the gas-phase oxidation over the catalyst resulting from the previous runs to evaluate the xylene isomers separately in the microreactor. The results clearly indicated that *p*-xylene was indeed preferentially oxidized to aldehydes while both *o*- and *m*-xylene remained almost intact. Encouraged by this result, the commercially available xylene feed containing ethylbenzene (15–20%) was tried [65]. The reactivity of ethylbenzene over the catalyst lies between that of *p*-xylene and *o*-xylene:

p-xylene ≫ ethylbenzene > *o*-xylene > *m*-xylene.

The results shown in Fig. 7 showed that the conversions of ethylbenzene, *o*-xylene and *m*-xylene remained low at a lower temperature (350°C), but increased to a substantial level at higher temperature (above 400°C).

3.3.4. *Silica-coated catalyst,* SiO_2/CVD Fe/Mo/*DBH*

It has been reported that the external pore size of ZSM-5 can be controlled by depositing $Si(OCH_3)_4$ by the CVD technique. Since the molecular sizes of $Si(OCH_3)_4$ and ZSM-5 pore size are estimated to be approximately 0.89 and 0.54×0.56 nm, respectively, only external pores are coated while the interior pores remain intact by the CVD process of $Si(OCH_3)_4$. The number of the cation sites are calculated to be 8.91 nm^{-2} by the external surface area of ZSM-5, it requires at least 4–6 layers of SiO_2 to control the pore size assuming the silica is coated completely in layers [5].

In order to improve the separation of *p*-xylene, an effort to enhance the para-selective property of the calcined CVD Fe/Mo/DBH catalyst was made by injecting a selectivating agent, $Si(OCH_3)_4$, in situ into the reactor, and the resulting catalyst contained approximately 1.4 wt% silica. As shown in Fig. 8, the preferential oxidation of *p*-xylene was noticeably improved by keeping the conversion of *o*-, and

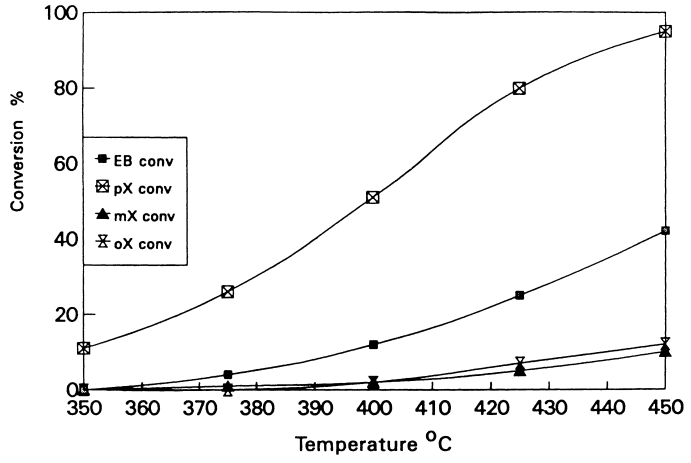

Fig. 7. The oxidation of xylene mixture with ethylbenzene over CVD Fe/Mo/DBH.

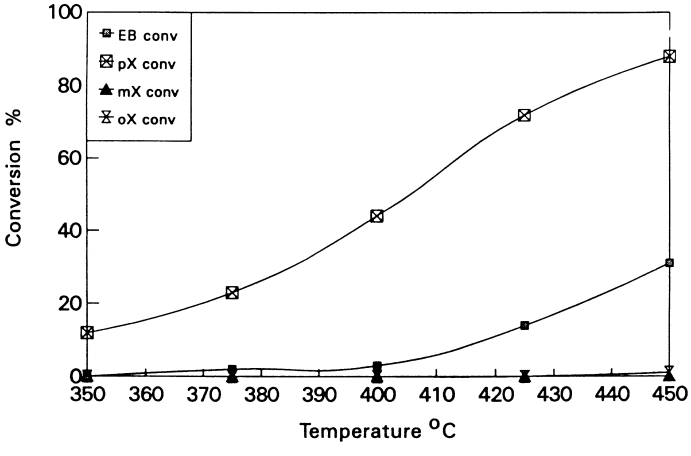

Fig. 8. The oxidation of xylene mixture with ethylbenzene over the silica-coated CVD Fe/Mo/DBH.

m-xylene and in particular ethylbenzene negligibly low [65,66]. The same silica-coated catalyst was also investigated for the oxidation of pure *p*-xylene under similar reactor conditions, and selectivities toward terephthaldehyde and *p*-tolulaldehyde were plotted against those for uncoated counterparts as a function of temperature in Fig. 9 and 10, respectively. The results show that the silica-coated catalyst provides better selectivity to terephthaldehyde, and consequently gives poorer selectivity for *p*-tolualdehyde over its uncoated counterpart. One drawback of the silica-coated catalyst is that it seems to burn

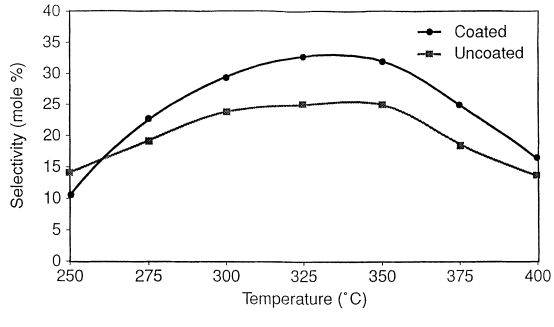

Fig. 9. Terephthaldehyde selectivity over CVD Fe/Mo/DBH and its silica-coated counterpart.

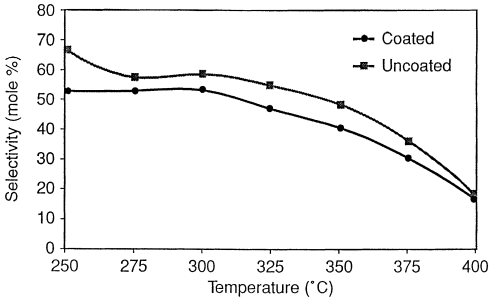

Fig. 10. *p*-Tolualdehyde selectivity over CVD Fe/Mo/DBH and its silica-coated counterpart.

the substrate more than the original uncoated catalyst.

3.3.5. *Effect of* CO_2

In the course of studying carbon dioxide as a burning suppressant for the gas-phase O_2 oxidation of alkylaromatics, it was unexpectedly found that the O_2 oxidation reaction was promoted in the presence of carbon dioxide over the CVD Fe/Mo/DBH catalyst [66]. The substrates included *p*- and *o*-xylene, and *p*-ethyltoluene. The conversion of these substrates to the corresponding aldehydes and other oxygenates was dramatically increased at low temperatures in the gas stream containing oxygen in CO_2.

The results for the gas-phase O_2 oxidation of *p*-xylene in the copresence of CO_2 are summarized in Table 5, and the *p*-xylene conversion and terephthaldehyde yield are plotted in Fig. 11 and 12, respectively. Much lower temperature was required to achieve the same level of *p*-xylene conversion in the presence of O_2 in CO_2 than in O_2 alone. The CO_2 molecules may be activated on the surface of CVD Fe/Mo/DBH catalyst to form the peroxocarbonate intermediate, $CO_4^=$, which may serve as a pro-

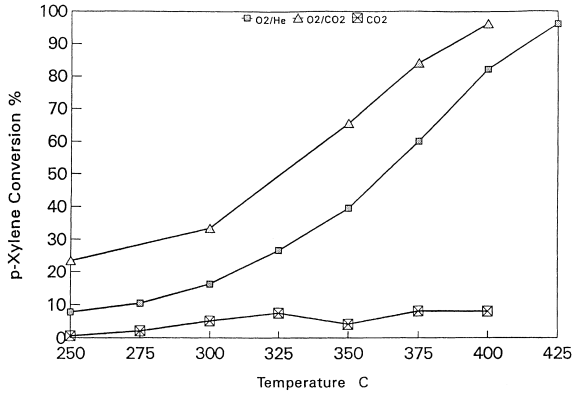

Fig. 11. Effect of CO_2 on the *p*-xylen conversion in the gas-phase O_2 oxidation over CVD Fe/Mo/DBH.

Table 5
Oxidation of *p*-xylene over CVD Fe/Mo/DBH with or without CO_2

	Temp. (°C)							
	300		325		350		375	
	Feed 1	Feed 2	Feed 1	Feed 2	Feed 1	Feed 2	Feed 1	Feed 2
p-Xylene vonv (%)	22.1	40.2	37.7	61.6	57.0	82.5	77.3	95.6
Product selectivity[a] (mol%)								
TOAL	51.8	48.3	47.5	41.8	40.1	33.1	30.5	20.3
TPAL	35.8	38.8	42.0	40.0	40.8	34.6	43.2	22.2
BZAL	2.3	2.3	3.4	3.0	4.2	3.7	4.7	3.8
MA	0	0	0	0.5	3.2	11.5	7.9	27.5
TOL	7.7	8.1	6.1	7.4	5.7	8.6	5.4	8.1
PCUMENE	0.4	0.4	0.1	0.1	0	0	0	0
TMBPM	3.2	2.2	1.7	0.9	0.9	0	0.3	0
CO	0	0	0	3.3	3.3	17.0	5.7	17.0
CO_2	0	0	—	0	—	9.4	—	

Feed gas 1: 0.1% *p*-xylene, 1.0% O_2, 1.0% N_2 in He.
Feed gas 2: 0.1% *p*-xylene, 1.0% O_2, 1.0% N_2 in CO_2.
Oxidation conditions: WHSV: 0.22 h^{-1}, contact time: 0.21 s, gas flow rate: 400 sccm.
[a]TOAL: *p*-tolualdehyde; TPAL: terephthaldehyde; BZAL: benzaldehyde; MA: maleic anhydride; TOL: toluene; PCUMENE: pseudocumene; TMBPM: trimethylbiphenylmethane.

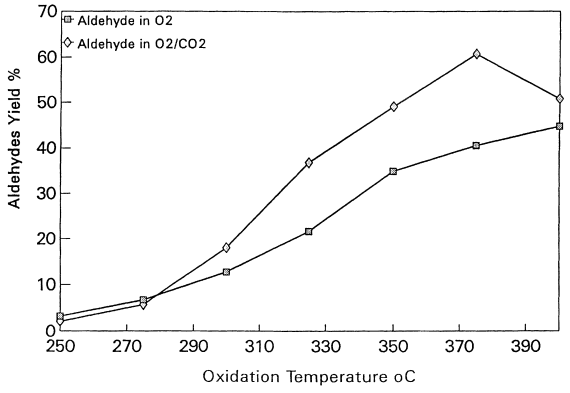

Fig. 12. Effect of CO_2 on the aldehyde yield in the gas-phase O_2 oxidation of *p*-xylene over CVD Fe/Mo/DBH.

moting species for the gas-phase O_2 oxidation reaction.

In the presence of CO_2, a dramatic improvement in the catalytic performance was observed in the oxidative catalytic dehydrogenation of ethylbenzene to styrene, but the presence of CO_2 adversely affected the oxidation of styrene to oxygenates in the subsequent oxidation step [67]. It appears that carbon dioxide promotes the hydrogen abstraction reaction occurring in the initial step of the oxidation process before the resulting alkenylaromatics are further oxidized to aldehyde/oxygenates at the subsequent oxidation step.

3.3.6. *Para-selective oxidation of polymethylated aromatics*

A series of methylaromatics was studied over the chemical vapor deposited M/Mo/DBH catalyst, CVD M/Mo/DBH (M=Fe, Sb, An, Bi, Zr or Sn). Methylaromatics include toluene, xylenes, pseudocumene, mesitylene and durene [68]. These catalysts exhibited a unique property of catalyzing oxidation of two para-oriented methyl substituents in the substrates to form terephthaldehyde derivatives. The para-oriented methyl substituents play a key role in defining the catalytic activity and selectivity toward aldehyde. Terephthaldehyde and monaldehyde derivatives were produced from *p*-xylene, pseudocuemen and durene while toluene was converted to benzaldehyhde, *m*-xylene and mesitylene remained unreactive over these catalysts. It seems that the reactivity of these substrates appear to be in the order *p*-xylene>durene>*o*-xylene>pseudocuemene>toluene>*m*-xylene>mesitylene. Both 2,6-dimethylnaphthalene and 4,4′-dimethyl-biphenyl were converted to monoaldehyde derivatives, 2-methyl-6-formylnaphthalene and 4-methyl-4′-formylbiphenyl, respectively.

3.3.7. *Effects of para-substituents in toluene derivatives*

The effects of various para-substituents in *p*-CH_3-C_6H_4-X (X stands for OH, OCH_3, CHO, C_2H_5, vinyl and Cl) were investigated in order to understand the para-selective nature of the CVD Fe/Mo/DBH [69]. The para-substituents such as OH, OCH_3 and Cl favorably influenced the oxidation of the methyl group to the corresponding aldehydes, OHC-C_6H_4-X. The CHO and C_2H_5 groups themselves were preferentially oxidized to form CH_3-C_6H_4-COOH and CH_3-C_6H_4-$CH{=}CH_2$, respectively, over the methyl group. In the same manner, the vinyl group was rapidly oxidized to oxygenates while the methyl group remained intact.

p-Methylanisole was oxidized to a sole product, *p*-anisaldehyde at 300°C. Selectivity to *p*-anisaldehyde and to CO_x were 81% and 15%, respectively. It is expected that burning occurring in the reaction can be suppressed by adding CO_2 and/or steam to the O_2 oxidation reactor. On the other hand, the very reactive *p-cresol* case was different. Selectivities toward *p*-hydroxybenzaldehyde, an expected product, phenol and CO_x were 14.1%, 5.5% and 80.5%, respectively. One can confirm that the catalyst is capable of oxidizing the methyl group in a para-position to the hydroxy group with extensive burning.

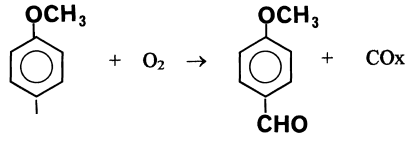

The CHO group in *p-tolualdehyde* was oxidized to produce *p*-toluic acid, and then further to maleic anhydride, but terephthaldehyde was formed in a very limited level. The ethyl group in *p*-ethyltoluene was initially converted to the vinyl group via oxidative dehydrogenation, which was further oxidized to aldehydes and ketone, and then to acid while the methyl group remained intact (see Table 6).

The oxidation of *styrene* was studied to gain some insight into the promoting effect of CO_2 observed with the substrates such as methyl- and alkyl-aromatics.

Table 6
Oxidation of *p*-ethyltoluene over CVD Fe/Mo/DBH

	Temp. (°C)					
	350		375		450	
	Feed 1	Feed 2	Feed 1	Feed 2	Feed 1	Feed 2
Conv. (%)	4.7	11.9	39.0	69.9	70.0	81.1
Selectivity (%)						
p-Methylstyrene	14.7	19.4	7.3	6.3	2.7	2.8
p-Toludldehyde	14.8	2.5	17.2	20.0	16.7	22.6
p-Me-acetophenone	5.6	8.4	6.9	6.7	5.6	6.7
p-Toluic acid	23.0	29.0	23.0	34.8	15.8	21.3
Terephthaldehe	0.3	0.8	0.6	1.2	1.3	2.4
CO	12.9	14.4	14.8	22.0	19.1	28.9
CO_2	24.6	24.9	29.8			

Feed 1: 0.16% *p*-ET (3.5 g/h), 5.5% O_2, 20% N_2 in He.
Feed 2: 0.16% *p*-ET (3.5 g/h), 5.6% O_2, 20% N_2 in CO_2.
WHSV: 0.36–0.37 h^{-1}, contact time: 0.21 s.

Table 7
Oxidation of styrene over CVD Fe/Mo/DBH

	Temp. (°C)					
	275		300		325	
	Feed 1	Feed 2	Feed 1	Feed 2	Feed 1	Feed 2
Conversion (%)	14.4	12.3	34.5	25.6	73.3	51.5
Product selectivity (%)						
Benzaldehyde	22.2	24.0	19.9	21.7	18.9	21.2
Phenylenylacetaldehyd	3.4	4.2	1.9	2.5	0.9	1.5
Acetophenone 9.2	9.7	6.5	7.7	3.8	5.2	
Benzoic acid	53.4	56.6	57.3	60.5	58.8	62.5
CO	6.3	5.5	6.6	5.7	7.9	6.2
CO_2	5.5	5.6	5.9			

Feed 1: 0.17% styrene, 5.0% CO_2, 18.3% N_2 in He.
Feed 2: 0.17% styrene, 5.0% O_2, 18.4% N_2 in CO_2.

Contrary to the methyl- and alkyl-aromatics, the presence of CO_2 adversely affected the oxidation of styrene (see Table 7). This finding contradicts the results observed in the liquid phase O_2 oxidation of styrene with iron- and Rh-complex catalysts [70]. As briefly stated in Section 3.3.6, the role of CO_2 played over the CVD Fe/Mo/DBH catalyst is to favorably influence the initial abstraction of hydrogen atoms from the methyl, ethyl or higher alkyl group in the alkylaromatiac substrates. Since the hydrogen abstraction step is the rate-determining step, the beneficial promoting effect of CO_2 on the overall reaction becomes remarkable. However, it seems that CO_2 does not participate in the subsequent oxidation of the resulting unsaturated alkenyl group to oxygenates such as aldelhyde, ketone and acid.

p- and m-Chlorotoluene were oxidized over the CVD Fe/Mo/DBH catalyst under the similar conditions, and were converted to the corresponding chlorobenzaldehyde [70]. In a typical run, 28% of *p*-chlorotoluene was converted to form mainly *p*-chlorobenzaldehyde in 61.6% selectivity at 325°C, while *m*-chlorotoluene was reacted (10.8%) at 350°C to *m*-chloro- and *p*-chlorobenzaldehyde in selectivities of

26.1% and 23.6%, respectively. As was expected, the *p*-chloro-substituted substrate, *p*-chlorotoluene, was much more reactive than its *m*-chlorotoluene counterpart. Contrary to the *p*-xylene oxidation, it is intriguing to observe that *m*-chlorotoluene is reactive to produce *p*-chlorobenzaldehyde in addition to the expected *m*-chlorobenzaldehyde, and that at elevated temperatures, 400–450°C, the yield of *p*-chlorobenzaldehyde surpasses that of *m*-chlorobenaldehyde. This finding suggests that *m*-chlorotoluene may be isomerized to *p*-chlorotoluene, and the isomerization reaction may become faster at higher temperatures. However, this does not necessarily rule out the possibility that *m*-chlorobenzaldehyde may be isomerized to *p*-chlorobenzaldehyde. *o*-Chlorobenzaldehyde was not detected in the oxidation runs with either *p*- or *m*-chlorotoluene.

3.3.8. Oxidative dehydrogenation of alkylaromatics

If an alkyl group in alkylaromatics is ethyl or higher, it was dehydrogenated to form an alkenyl group at the initial step when these substrates were subjected to the gas-phase O_2 oxidation over the CVD Fe/Mo/DBH catalyst under the normal oxidation conditions. The resulting alkenyl group was much more reactive than the substrate itself, and it was difficult to stop at the alkenyl stage unless the reaction temperature was maintained at a low temperature. Consequently, it was immediately oxidized to aldehyde, ketone and carboxylic acid by the subsequent oxidation [71].

Ethylbenzene (EB), *p*-ethyltoluene (ET) and diethylbenzene (DB) were chosen to demonstrate the three functions expected from the O_2 oxidation over the catalyst. The three functions include para-selective property, the initial oxidative dehydrogenation precedes the oxygenation reaction, and CO_2 promoting effect [66].

These three substrates were subjected to the gas-phase O_2 oxidation over the CVD Fe/Mo/DBH catalyst under the reaction conditions described in Table 8. Since considerable exothermicity was observed with *p*-diethylbenzene, the reactor temperature was lowered and the flow rate of the feed was increased double in this study. This observation led us to conclude that *p*-diethylbenzene was far more reactive than ethylbenzene, *p*-ethyltoluene, and *p*-xylene.

Table 8
Gas-phase O_2 oxidation of ethylbenzene (EB), *p*-ethyltoluene (ET) and *p*-diethylbenzene (DEB)

	Substrate			
	EB		ET	DEB
Temp. (°C)	325	375	375	325
Conversion (%)	5.2	22.6	39.0	27.1[a]
Product selectivity (%)				
Styrene	25.3	7.1		
Benzaldehyde	37.9	28.1		
Benzoic acid	11.6			
Maleic anhydride		24.7		
CO	10.7	12.1	14.8	
CO_2	24.4	17.8	24.9	
p-Methylstyrene			7.3	
p-Tolualdehyde			17.2	
p-Toluic acid			23.0	
p-Methylacetophenone			6.9	
Terephthaldehyde			0.6	
o-Diethylbenzene[b]				10.0[c]
p-Divinylbenzene				1.6
Terephthaldehyde				17.3
p-Vinylbenzaldehyde				5.5
p-Ethylstyrene				26.6
p-Ethylbenzaldehyde				7.7
p-Ethylbenzoic acid				26.3
Unidentified products				4.1

Reaction conditions: for ET, WHSV: 0.57 h^{-1}, feed: 6% O_2, 6% N_2 in He, flow rate: 400 sccm, O_2/ET: 7.51/1; for DEB, feed: 6% O_2, 6% N_2 in He, flow rate: 800 sccm.
[a]Area %.
[b]May be the isomerization product of *p*-diethylbenzene or impurity.
[c]Excluding CO_2, *p*-diethylbenzene (DEB).

Two dehydrogenation products, *p*-ethyl- styrene and *p*-divinylbenzene, were initially formed at two different active sites, e.g., ''single'' and ''pair'' site, respectively, from the *p*-diethylbezene substrate [4], and these resulting alkenylbenzene products were subsequently further oxidized via two different reaction paths, as shown in the illustration given in Section 3.1.4. *p*-Ethylstyrene was converted to *p*-ethylbenzalehyde and then to *p*-ethylbenzoic acid while much more reactive *p*-divinylbenzene was quickly oxidized to *p*-vinylbenzaldehyde and then to terephthaldehyde.

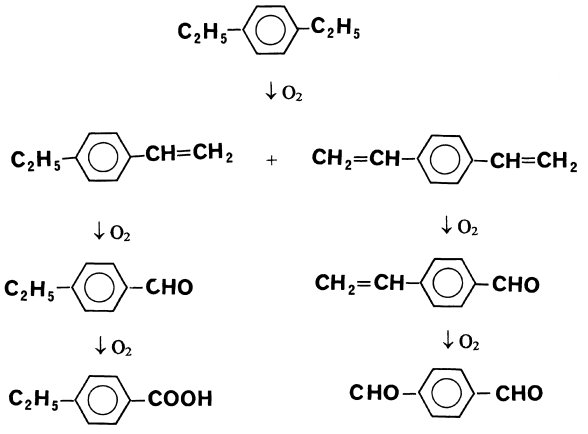

Based on the reaction mechanism postulated on the *p*-xylene oxidation [4], it was theorized that the oxidative dehydrogenation of the ethyl group in the *p*-diethylbenzene substrate must occur in two ways, using the ''single'' site or the ''pair'' sites for the catalyst. If just one ethyl group in *p*-diethylbenzene interacted with the ''single'' site of the catalyst in the stand-on manner, *p*-ethylstyrene was produced as a result of single α,β-hydrogen elimination reaction. Once *p*-ethylstyrene was formed, the second ethyl group became much more difficult to be oxidized, and rather the vinyl group in *p*-ethylstyrene was oxidized further to *p*-ethylbenzaldehyde, which eventually converted to *p*-ethylbenzoic acid. On the other hand, if two ethyl groups in *p*-diethylbenzene interacted in a concerted manner on the ''pair'' sites of the catalyst in the lying-on fashion, *p*-divinylbenzene was formed as a result of the concerted double α,β-hydrogen elimination reactions at the two ethyl groups. *p*-Divinylbenzene was extremely reactive and converted to terephthaldehyde and *p*-vinylbenzaldehyde upon the subsequent oxidation. The analysis of the product distribution listed in Table 8 reveals that the ''single'' site path favors approximately more than 2:1 (60.6%:24.4%) ratio over the ''pair'' sites path under the reaction conditions employed in this work. The promoting effect of CO_2 was also observed in the oxidation of *p*-ethyltoluene (see Table 9).

3.3.9. Oxidative dehydrogenation of alkanes

Low alkanes such as *n*-butane, propane and ethane were subjected to the gas-phase O_2 oxidation in a reactor under the conditions employed for the alkylaromatics oxidation [71]. *n*-Butane was oxidized in a quartz reactor loaded with 10 g of the CVD Fe/Mo/DBH catalyst. A premixed feed containing 0.5% *n*-butane, 28% O_2 and 3% N_2 in CO_2 was used for the oxidation. The *n*-butane substrate was converted to maleic anhydride, and an anticipated dehydrogenated intermediate, *n*-butene, was not detected in the reaction effluent.

The premixed gases consisting of 2% propane (or ethane), 4% O_2 and 4% N_2 in He were subjected to the oxidation reaction in the quartz reactor loaded with 5.0 g of CVD Zr/Mo/DBH catalyst, which was prepared from $ZrCl_4$, MoO_2Cl_2 and borosilicate molecular sieve by the CVD method. The results combined in Table 10 show that *n*-butane was converted to maleic

Table 9
Oxidation of *p*-ethyltoluene over CVD Fe/Mo/DBH (a regular reactor loaded with 10 g catalyst)

	Temp. (°C)					
	350		375		400	
	Feed 1	Feed 2	Feed 1	Feed 2	Feed 1	Feed 2
Conversion (%)	4.7	11.9	39.0	60.0	70.0	81.1
Product selectivity (%)						
p-Methylstyrene	14.7	19.4	7.3	6.4	2.7	2.8
p-Tolualdehyde	14.8	22.5	17.2	20.0	16.7	22.6
p-Me-acetophenone	5.6	8.4	6.9	6.7	5.6	6.7
p-Toluic acid	23.0	29.0	23.0	34.8	15.8	21.3
Terephthaldehyde	0.3	0.8	0.6	1.2	1.3	2.4
CO	12.9	14.4	14.8	22.0	19.1	28.9
CO_2	24.6		24.9		29.8	

Feed 1: 0.16% ET, 5.5% O_2, 20% N_2 in He.
Feed 2: 0.16% Et, 5.6% O_2, 20% N_2 in CO_2.

Table 10
Oxidation of *n*-butane over CVD Fe/Mo/DBH, propane and ethane over CVD Zr/Mo/DBH

	Alkane oxidant					
	n-Butane O_2 in CO_2		Propane O_2		Ethane O_2	
Temp. (°C)	400	425	500	550	550	600
Conversion (%)	14.5	34.0	3.9	10.3	2.0	3.8
Product selectivity (%)						
Ethylene			0.2	0.6	88.5	86.3
Propylene			85.2	70.3		
Maleic anhydride	8.9	3.7				
CO	91.4	96.3	10.4	21.0	11.0	13.0
CO_2			3.7	4.7		

anhydride in a stream of O_2 in CO_2, while propane and ethane were oxidatively dehydrogenated to propylene and ethylene, respectively, over the CVD Zr/Mo/DBH catalyst.

3.4. *Effect of supporting matrix*

ZSM-5. The CVD Fe/Mo/supporting matrix (ZSM-5, silicalite, Y-zeolite, mordenite, β-zeolite) was investigated to define the role of the partially deboronated borosilicate molecular sieve (DBH) for the gas-phase O_2 oxidation of *p*-xylene [72]. The DBH matrix played a unique role for the selective synthesis of aldehydes, terephthaldehyde and *p*-tolualdehyde, from the gas-phase O_2 oxidation. Terephthaldehyde was produced over CVD Fe/Mo/DBH, while disproportionation of *p*-xylene became predominant over CVD Fe/Mo/ZSM-5. The CVD Fe/Mo/silicalite catalyst, containing low levels of iron (0.14 wt%) and molybdenum (0.50 wt%), was active for aldehyde synthesis, but a significant extent of side reactions and extensive burning accompanied the oxidation reaction. This is mainly due to restricted number of the silanol, Si-OH, available on the dealuminated silicalite surface. The different catalytic behaviors observed on these three catalysts with DBH, ZSM-5 and silicalite were explained by the results of Raman spectroscopy and electron micrography. Significant destruction of the molecular sieve structure occurred in the ZSM-5 and silicalite matrix during the CVD process [4,72].

Other zeolite matrices such Y-zeolite, mordenite, and β-zeolite and their dealuminated counterparts were investigated for the same *p*-xylene O_2 oxidation under comparable reaction conditions. These results indicate that the ZSM-5 matrix is the best among these matrices, but the DBH matrix is much more active and selective for the aldehyde synthesis. Since these two matrices have the identical MFI structure, a further study was conducted to find out what causes the observed different catalytic behaviors.

CVD Fe/Mo/ZSM-5 (catalyst 1) catalyst was prepared from $FeCl_3$ and ZSM-5 (Si/Al=30) containing 1.07 wt% Al, and its composition was 5.3, 2.21 wt% Fe, atomic ratio of Mo/Fe=1.4/1. In order to increase the Mo/Fe ratio above 1.5/1, which is a stoichiometry of $Fe_2(MoO_4)_3$, an aqueous solution of ammonium paramolybdate was impregnated onto catalyst 1 by the incipient wetness technique. The resulting catalyst (referred to as catalyst 2) contained 8.9 wt% Mo, 2.47 wt% Fe, and the Mo/Fe ratio=2.0.

Raman spectra shown in Fig. 13 for catalyst 1 and Fig. 14 for catalyst 2 indicates that catalyst 2 displayed a much diminished α-Fe_2O_3 band and a much greater amount of MoO_3 relative to $Fe_2(MoO_4)_3$ than catalyst 1. Some portion of impregnated ammonium paramolybdate must have interacted with α-Fe_2O_3 to form $Fe_2(MoO_4)_3$, while the remaining portion was retained on the ZSM-5 surface to form MoO_3 after calcination. Although the α-Fe_2O_3 phase was virtually absent in catalyst 2 sample, disproportionation and oxidative dehydrcoupling of the *p*-xylene substrate persisted with a limited formation of aldehydes. The results are summarized in Table 11.

The results in Table 11 show that the main reaction over catalysts 1 and 2 is disproportionation of *p*-xylene to toluene and pseudocumene, and dehydrocoupling of *p*-xylene to trimethylbiphenylmethane with sub-

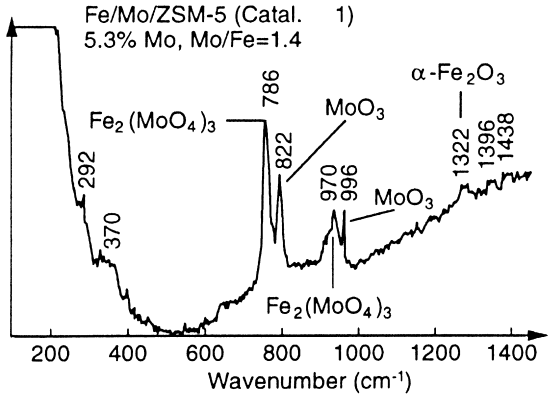

Fig. 13. Raman spectrum of CVD Fe/Mo/ZSM-5, catalyst 1.

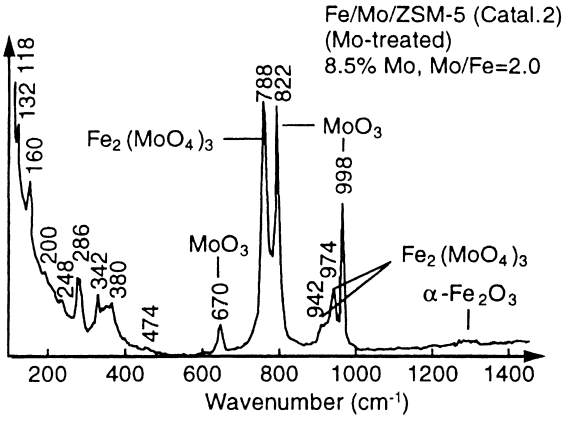

Fig. 14. Raman spectrun of CVD Fe/Mo/ZSM-5, catalyst 2.

Table 11
Gas-phase O_2 oxidation of *p*-xylene over Fe/Mo/ZSM-5

	Catalyst 1			Catalyst 2				
	Temp. (°C)			Temp. (°C)				
	300	350	400	325	350	375	400	425
Conversion (%)	26.6	58.0	94.9	24.0	42.5	61.0	77.4	95.0
Product selectivity (mol%)								8.1
Terephthaldehyde				20.0	20.9	16.8	13.8	8.1
p-Tolualdehyde	0	2.5	0.9	6.4	6.4	5.9	7.0	6.1
Benzaldehyde	3.9	0.8	1.3	0.3	0.1	0.1		
Toluene	53.1	62.0	33.9	39.4	35.4	33.5	24.3	17.6
Pseudocumene	15.1	3.7	0	3.6	1.9	1.0	0.3	0
TMBPM[a]				8.2	4.1	1.4	0.3	0
CO				0	8.1	11.9	14.0	18.2
CO_2				21.0	21.5	26.1	34.0	38.9
$CO+CO_2$	26.5	28.4	47.2					

Catalyst 1: 5.53 wt% Mo, 2.21 wt% Fe, Mo/Fe=1.4.
Catalyst 2: 8.5 wt% Mo, 2.47 wt% Fe, Mo/Fe=2.0.
Gas stream: 0.1% *p*-xylene, 1.0% O_2, 2.0% N_2 in He.
[a]Trimethylbiphenylmethane.

stantial burning. However, catalyst 2 produced some aldehydes, and the selectivities to terephthaldehyde and *p*-tolualdehyde were, respectively, 21% and 6.4% at 24–43% conversion of *p*-xylene at 325–350°C. The aldehyde yields were much lower than those over CVD Fe/Mo/DBH. These results bring out a unique role played by the DBH matrix in contrast to ZSM-5 and other zeolitic matrices for the *p*-xylene oxidation.

Deboronated borosilicate molecular sieve (*DBH*). It has been known that the acidity of the borosilicate molecular sieve, HAMS-3B-3, is related to the boron content remaining in the framework. In general, stronger acidity is generated as the boron content decreases in the DBH matrix. Two samples of DBH 1 containing 1.0 wt% boron and DBH 2 containing 52 ppm boron were prepared from the HAMS-1B-3 containing 1.70 wt% by a normal ion exchange with an aqueous ammonium acetate solution in a beaker and a continuous exchange process using a Soxhlet extractor, respectively. The resulting samples were evaluated for the gas-phase O_2 oxidation of *p*-xylene with or without CO_2. The results are summarized in Table 12.

Table 12
The *p*-xylene oxidation over DBH 1 and DBH 2

	Temp. (°C)						
	300		350			400	
	Catalyst DBH		Catalyst DBH			Catalyst DBH	
	1	2	1	2	3[a]	1	2
p-Xylene conv. (%)	14.8	16.4	18.5	20.1	65.5	28.0	26.1
Product selectivity (%)							
Toluene	54.4	42.8	48.4	48.7	4.8	44.3	54.3
Pseudocemene	9.4	13.5	4.5	8.7	0	1.4	4.5
Benzaldehyde					2.7	1.7	0.8
p-Tolualdehyde	25.5	16.3	28.2	20.9	40.9	19.6	18.2
Terephthaldehyde	0	0	0	0	33.6	0	0
Benzoic acid	0	0	0	0	0	14.3	4.9
TMBPM[b]	10.7	27.4	5.0	21.7	1.6	0.9	1.5
CO	0	0	14.0	0	3.6	17.6	20.7
CO_2					15.6		

Feed: 0.1% *p*-xylene, 1.0% N_2, and 1.0% O_2 in CO_2.
[a]CVD Fe/Mo/DBH containing 540 ppm B.
[b]Trimethylbiphenylmethane.

Disproportionation of *p*-xylene to toluene and pseudocumene, and dehydrocoupling of *p*-xylene to trimethylbiphenylmethane are principal reactions over these DBH 1 and 2. The selectivity to toluene and pseudocumene, disproportionation products of *p*-xylene, were higher with DBH 1 than DBH 2. However, trimethylbiphenylmethane, an oxidative dehydrocoupling product of *p*-xylene, was significantly higher with DBH 2 than DBH 1.

As was expected, terephthaldehyde was not found in the product of these runs, but it was very surprising to observe *p*-tolualdehyde in the product in a substantial amount in a feed stream containing O_2 in CO_2. The reaction mechanism how *p*-tolualdehyde is formed on the DBH surface without metal component is not understood, and it is also not clear whether or not the *p*-tolualdehyde produced over CVD Fe/Mo/DBH is partially contributed by the DBH matrix itself. It is therefore speculated that, besides the ''single'' site on the ferric molybdate phase, the deboronated borosilicate molecular sieve matrix itself may be involved in the oxidation reaction for the *p*-tolualdehyde formation.

3.5. Ag^+-*doped CVD* Fe/Mo/*DBH*

The Ag^+-doped CVD Fe/Mo/DBH catalyst was prepared by impregnating an aqueous $AgNO_3$ solution onto the CVD catalyst Fe/Mo/DBH catalyst via the incipient wetness method. In short, Ag/Fe/Mo/DBH was prepared by a combination of the CVD technique and the conventional impregnation method. By doping Ag^+ in a level of 760 ppm, significant changes in the surface property and catalytic behavior occurred. The surface area was dramatically reduced to 169 from 256 m^2/g for the original CVD Fe/Mo/DBH catalyst. This change was reflected on a noticeable decrease in the catalytic activity, e.g. the *p*-xylene conversion. At the same time, the side reactions catalyzed by the acid sites of the DBH matrix, namely disproportionation and dehydrocoupling of the *p*-xylene substrate, were completely suppressed, and the ''pair'' sites contributing to the formation of terephthaldehyde were effectively poisoned. Thus, *p*-tolualdehyde was produced as a predominant sole oxygenate product in a high selectivity [73]. The data summarized in Table 13 clearly support these conclusions.

3.6. N_2O *oxidation of benzene to phenol*

Direct hydroxylation of benzene to phenol has long been sought as a desirable process over the conventional cumene oxidation process. Nitrous oxide, N_2O, can be an attractive active oxygen source for a variety of oxidation reactions because it is thermodynami-

Table 13
Gas-phase O_2 oxidation of *p*-xylene over Ag/Fe/Mo/DBH

	Catalyst					
	Ag-doped		Fe/Mo/DBH		DBH 2	
B content					1.0%	52 ppm
Surface area (m^2/g)	169		256		348	403
Temp. (°C)	350	350	350	350	350	350
Feed type	1	2	1	2	2	2
p-xylene conv. (%)	13.6	32.3[a]	41.2	65.5[a]	3.8[a]	18.5[a]
Product selectivity (%)						
p-Tolualdehyde	79.3	90.7	50.2	60.5	28.2	20.9
Terephthaldehyde	1.0	2.6	23.5	33.6	0	0
Benzaldehyde	0.4	0.4	2.4	2.7	0	0
Maleic anhydride	0	0	3.2	11.5	0	0
Toluene	0.8	1.2	3.5	4.8	48.4	48.7
Trimethylbiphenylmethane	0	0.1	1.7	0.6	5.0	21.7
CO	0	4.9	0.6	3.2	14.0	0
CO_2	18.5	—	15.6	—	—	—

Feed 1: 0.1% *p*-xylene, 1.0% O_2, 1.0% N_2 in He.
Feed 2: 0.1% *p*-xylene, 1.0% O_2, 1.0% N_2 in CO_2.
[a]Conversion and selectivity including CO_2.

cally unstable, and kinetically inert in the absence of an activating center. Both CVD Fe/Mo/DBH and its impregnated counterpart were studied along with the silica gel coformed catalyst, Fe/Mo/SiO_2, for the hydroxylation of benzene to phenol with N_2O. The results summarized in Table 14 and plotted in Fig. 15 indicate that the CVD catalyst was active for the reaction while its impregnated counterpart exhibited lower catalytic activity. The gel coformed catalyst displayed practically no activity [74].

Aqueous solutions of ammonium paramolybdate and ferric nitrate were added slowly and simultaneously into Nalco silica gel 1034A containing 34% silica under vigorous agitation at 80–85°C for several hours. The system was allowed to cool down, and was kept at an ambient temperature overnight. Water was removed by a rotary evaporator or microwave oven, and the catalyst was dried in a microwave or vacuum oven and calcined in air at 600°C for 5 h. A series of gel coformed M/Mo/SiO_2 (M=Fe, Bi, Sn, Zn, Zr, Ti)

Table 14
Comparison of N_2O oxidation of benzene to phenol

	Supporting matrix						
	DBH (CVD)		Fe/Mo/DBH (Impregnated)			Fe/Mo/SiO_2 (Gel coformed[a])	
	Temp. (°C)		Temp. (°C)			Temp. (°C)	
	350	410	335	385	400	335	335–410
Benzene conv. (%)	8	17	2	9	5	0.2	0.5
Product selectivity (%)							
Phenol	~100	97	100	~100	~100	~100	~100
Unidentified	Trace	3					
Recovery (5)	90	84	96	82	91	94	88

Catalyst: CVD Fe/Mo/DBH, impregnated catalyst, gel coformed Fe/Mo/SiO_2.
[a]See Section 3.7.

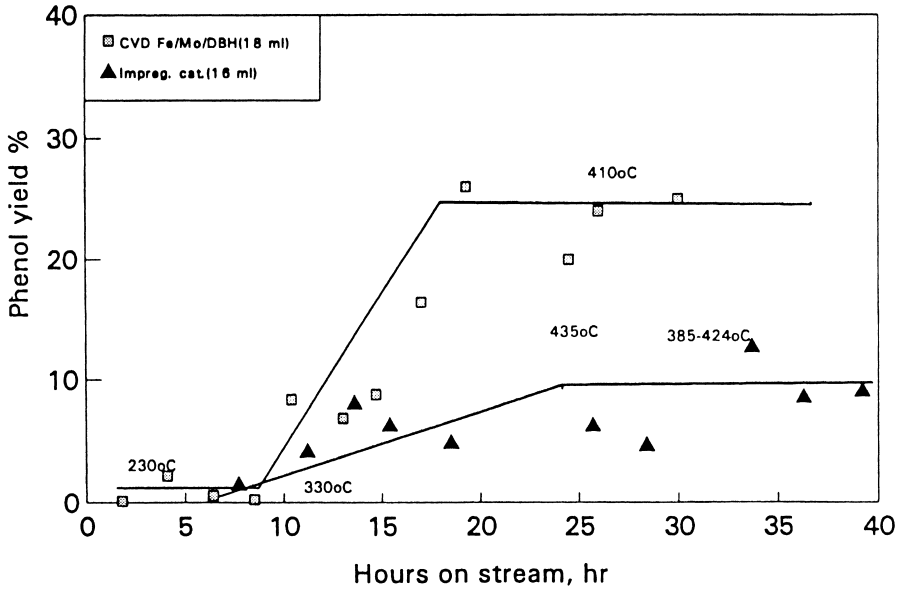

Fig. 15. Synthesis of phenol from benzene by N_2O oxidation, CVD Fe/Mo/DBH versus impregnated counterpart.

were prepared by using the same procedure, and evaluated for the nitric acid oxidation of benzene to phenol in the gas phase. The results led to the following ranking of these catalysts: Fe>Bi>Sn>Zn>Zr>Ti. In short, gel coformed $Fe/Mo/SiO_2$ catalyst was found to be the most active and selective to phenol by the nitric acid oxidation of benzene in the gas phase [75].

3.7. *Gel coformed* $Fe/Mo/SiO_2$

The gel coformed catalyst exhibited a dual function, selective formation of nitrobenzene and phenol in the nitric acid oxidation of benzene in the vapor phase. At lower temperatures (<370°C), nitrobenzene was formed selectively, and this function switched to the selective phenol formation above 400°C. In addition to the reaction temperature, the catalyst composition, in particular, the atomic ratio of Mo/Fe, appears to play an important role for defining the product selectivity [75].

The catalyst having Mo/Fe $\geq$1.5 consists of $Fe_2(MoO_4)_3$ phase alone, produces only phenol at all temperatures studied, 350–475°C. Nitrobenzene was converted to phenol over the catalyst under similar nitric acid oxidation condition.

The phenol yield was significantly improved by blending 1 mol% nitrobenzene in the benzene feed. Nitrobenzene in a dilute concentration serves as an effective promoter for the selective gas phase nitric acid oxidation of benzene to phenol.

3.8. *Aerogel catalysts*

Gel produced via solution–sol–gel method can be classified into three categories, e.g., aerogel, xerogel and cryogel, depending on the technique to remove the solvent in the system. The solvent is removed under the super critical condition to prepare aerogel, which assumes a uniform chemical composition having highly porous micro-structure, high surface area, and yet has excellent stability than the xerogel and cryogel counterpart prepared by the conventional methods. In other words, the aerogel technique not only improves the property of existing catalysts, but also provides very stable nano-size material. The superior property of aerogel is reflected on the better performance of various catalytic oxidation reactions.

3.9. *Aerogel* TiO_2/SiO_2

Aerogel TiO_2/SiO_2 not only improved the property of existing catalysts prepared by the conventional techniques, but also provided a very stable nano-size material. The superior property of the resulting aero-

gel is reflected on the better performance on various catalytic oxidation. Aerogel TiO_2/SiO_2 has been reported to be an excellent catalyst for epoxidation of I-hexene, cyclohexene, limonene, and norbornene with cumenehydroperoxide to the corresponding epoxides [76]. Various other aerogel catalysts have also been known to be more active than their conventional counterparts for different types of oxidation reactions: Aerogel SiO_2, Pt–SiO_2, NiO/SiO_2, Cr_2O_3, and Fe_2O_3 for oxidation of acetaldehyde to acetic acid, aerogel NiO/Al_2O_3, and $NiO/SiO_2/Al_2O_3$ for oxidizing 2-methylpropane to methylacrolein and acetone, aerogel CuO/Al_2O_3 for conversion of *n*-butane to furan and 1-butene to furan, crotonaldehyhde, acetic, and methyvinylketone, and finally, photoactivated aerogel TiO_2 for oxidation of paraffins and olefins [77].

An attempt to prepare better catalysts, which exhibit higher activity and better product selectivity, is being made via the complexing agent or surfactant assisted sol–gel method [78].

4. Conclusions

The oxidation and other interesting reactions catalyzed by a series of nano-structured single metal and bimetallic oxides catalysts prepared by the chemical vapor deposition (CVD) techniques were reviewed. Among the various matrices studied, such as borosilicate, ZSM-5, β-zeolite, mordenite, silicalite and Y-zeolite, the partially deboronated borosilicate molecular sieve (DBH) played a unique role for the para-selective oxidation of *p*-xylene. The CVD Fe/Mo/DBH catalyst activated by a proper calcination process maintained higher catalytic activity, better product selectivity, and superior catalytic stability in the selective formation of aldehydes, in particular, terephthaldehyde and *p*-tolualdehyde, over the impregnated counterpart, bulk catalytic moiety and the CVD catalyst deposited on different zeolite matrices, despite the unusually high surface area of 250–316 m^2/g as an oxidation catalyst.

The author focused mainly on the gas-phase O_2 oxidation of alkylaromatics over the CVD Fe/Mo/DBH displaying the para-selectivity, which was attributable to the molecular shape of the substrate, the molecular geometry of the active catalytic species, and characteristic pore structure.

The para-selective property of CVD Fe/Mo/DBH was improved by depositing the nano-sized silica on its external surface, namely selectivity toward terephthaldehyde was enhanced while that of *p*-tolualdehyde was correspondingly decreased for the *p*-xylene oxidation. This finding led to the conclusion that silicon alkoxides, $Si(OR)_4$, is indeed a good para-selectivating agent. In general, silica overlayer in nano-size deposited on zeolite by the CVD of silicon alkoxides provided useful functions: (1) control of the pore-opening of zeolite, (2) totally or selectively inactivate the surface, and (3) imparting the thermal stability and solid acidity to the basal plane.

CVD Fe/Mo/ZSM-5 oxidized *p*-xylene to produce aldehydes to a substantial extent, but disproportionation and dehydrocoupling of *p*-xylene to toluene and pseudocuemene, and trimethylbiphenylmethane, respectively, persisted throughout the runs. The intrinsic acidity of the DBH matrix itself is believed to be responsible for these side reactions. However, it is noteworthy to mention that *p*-tolualdehyde was observed with the DBH matrix itself, although it was a minor product, in the *p*-xylene oxidation in the stream containing both O_2 and CO_2. The unexpected promoting effect of CO_2 on the selective oxidation of alkylaromatics over CVD Fe/Mo/DBH and DBH is primarily stemmed from the initial H abstraction from the substrate. The CO_2 molecule may be activated on the catalyst surface to generate more mobile and active oxygen species than the molecular oxygen via a peroxocarbonate intermediate, $CO_4^=$ [70,79].

CVD Fe/Mo/silicalite, containing low levels of iron and molybdenum attributing to restricted number of the silanol group available on the silicalite surface, was also active for aldehyde synthesis, but a significant extent of side reactions and extensive substrate burning accompanied. These side reactions were completely suppressed by doping Ag^+ in a 760 ppm level on CVD Fe/Mo/DBH via the conventional incipient impregnation technique. But this process seems to poison the ''pair'' sites which are believed to be responsible for terephthaldehyde formation. Various other interesting reactions over the nano-sized single metal oxides on zeolite and other matrices are also reviewed.

It is expected that the interesting catalytic reactions will be discovered by expanding this work to the mesopore matrices via CVD deposition or encapsulation of the catalyst moiety inside the pore structure.

References

[1] W.R. Moser (Ed.), Advanced Catalysts and Nanostructured Materials, Modern Synthetic Methods, Academic Press, New York, 1996.
[2] H. Gleiter, Prog. Mater. Sci. 33 (1989) 22.
[3] J.Y. Ying, in: G.C. Hadjipanayis, R.W. Siegel (Eds.), Nanophase Materials: Synthesis–Properties–Applications, Kluwer, Dordrecht, 1994, p. 37.
[4] J.S. Yoo, J.A. Donohue, M.S. Kleefisch, P.S. Lin, S.D. Elfline, Appl. Catal. 105 (1993) 83; J.S. Yoo, J.A. Donohue, C. Choi-Feng, in: W.R. Moser (Ed.), Advanced Catalysts and Nanostructured Materials, Academic Press, New York, 1996, p. 453.
[5] Y. Iwasawa, Shokubai 37(4) (1995) 292.
[6] M. Niwa, Shokubai 38(1) (1996) 13.
[7] E.C. Alyea, K.F. Brown, K.J. Fisher, K.D.L. Smith, Proceedings of the 10th International Congress on Catalysis, Budapest, Elsevier, Amsterdam, 1993, p. 503.
[8] E.C. Alyea, K.F. Brown, K.J. Fisher, J. Mol. Catal. 64 (1990) L11.
[9] M. Baerns, S. Termath, M. Reiche, in: W.R. Moser (Ed.), Advanced Catalysts and Nanostructured Materials, Academic Press, New York, 1996, p. 479.
[10] K.S. Suslick, T. Hyeon, M. Fand, A.A. Cichowlas, in: W.R. Moser (Ed.), Advanced Catalysts and Nanostructured Materials, Academic Press, New York, 1996, p. 197.
[11] K.S. Suslick, Science 247 (1990) 1439.
[12] K.S. Suslick, Ultrasound: Its Chemical, Physical, and Biological Effects, VCH Publishers, New York, p. 123.
[13] D.W. Matson, J.C. Linehan, J.G. Darab, M.F. Buehler, M.R., Phelkps, G.G. Neuenschwander, in: W.R. Moser (Ed.), Advanced Catalysts and Nanostructured Materials, Academic Press, New York, 1996, p. 259.
[14] W.R. Moser, J.E. Sunstrohm IV, B. Maarshik-Guerts, in: W.R. Moser (Ed.), Advanced Catalysts and Nanostructured Materials, Academic Press, New York, 1996, p. 285.
[15] P.F. Miquel, J.L. Katz, in: W.R. Moser (Ed.), Advanced Catalysts and Nanostructured Materials, Academic Press, New York, 1996, p. 515.
[16] A.M. Buckley, M.J. Greenblatt, Chem. Edu. 71 (1994) 599.
[17] L.L. Hench, J.K. West, Chem. Rev. 90 (1990) 33.
[18] C.J. Brinker, G.W. Scherer, Sol–Gel Science, Academic Press, New York, 1989.
[19] M. Toba, Shokubai 36(5) (1994) 319.
[20] G. Centi, M. Marella, L. Meregalli, S. Perathoner, M. Tomaselli, T. La Torretta, in: W.R. Moser (Ed.), Advanced Catalysts and Nanostructured Materials, Academic Press, New York, 1996, p. 63.
[21] A. Wold, Y.-M. Gao, D. Miller, R. Kershaw, K. Dwight, in: W.R. Moser (Ed.), Advanced Catalysts and Nanostructured Materials, Academic Press, New York, 1996. p. 479.
[22] W.R. Moser, J.D. Lennhoff, J.E. Cnossen, K. Fraska, J.W. Schoonover, J.R. Rozak, in: W.R. Moser (Ed.), Advanced Catalysts and Nanostructured Materials, Academic Press, New York, 1996, p. 535.
[23] S. Niwa, J. Mizukami, M. Toba, R. Kutsuzawa, Sokubai 37(2) (1995) 140.
[24] S.B. Desu, J. Am. Chem. Soc. 79 (1989) 1615.
[25] K. Maeda, S.M. Fischer, Solid State Technol. (1993) 3.
[26] T. Nakajima, M. Matsuoka, S. Mishima, I. Matsuzaki, Nippon Kagaku kaishi 12 (1994) 1134.
[27] K. Ikeda, S. Nakayama, M. Maeda, Semicond. World (1994) 60.
[28] K. Fujino, Y. Nishimoto, N. Tokumasu, K. Maeda, J. Electrochm. Soc. 139 (1989) 79.
[29] T. Hattori, M. Matsuda, K. Suzuki, A. Miyamoto, Y. Murakami, Stud. Surf. Sci. Catal. 4 (1988) 1640.
[30] K. Inumaru, T. Okuhara, M. Misono, Chem. Lett. (1990) 1207.
[31] S. Sato, T. Sodesawa, F. Nozaki, Shokubai 32(6) (1990) 342.
[32] N. Katada, M. Niwa, Y. Murakai, Shokubai 32(2) (1990) 59.
[33] K. Inumaru, T. Okuhara, M. Misono, Shokubai 32(2) (1990) 51.
[34] J.S. Yoo, M.S. Kleefisch, J.A. Donohue, US Patent 5 324 702, 28 June 1994, Amoco.
[35] G.W. Zajac, C. Choi-Feng, J. Faber, J.S. Yoo, R. Patel, H. Hochst, J. Catal. 151 (1995) 338.
[36] E.F. Vansanat, Pore Size Engineering in Zeolites, Wiley, New York, 1990.
[37] M. Niwa, S. Kato, T. Hattori, Y. Murakami, J. Chem. Soc. Faraday Trans. 80 (1984) 3135.
[38] G. Peeters, A. Thys, P. Devievre, E.F. Vansant, Proceedings of the Sixth International Zeolite Conference, Reno, 1983, p. S-49.
[39] M. Niwa, M. Kato, T. Hattori, Y. Murakami, J. Phys. Chem. 90 (1986) 6233.
[40] T. Hibino, M. Niwa, Y. Murakami, J. Catal. 128 (1991) 551.
[41] H. Das, Y.S. Bhat, A.B. Halgeri, Ind. Eng. Chem. Res. 32 (1993) 2525.
[42] H. Kuno, M. Shibagaki, K. Takahashi, I. Honda, H. Matsushima, Proceedings of the 10th International Congress on Catalysis, Budapest, 1993, p. 1727.
[43] H. Kuno, M. Shibagaki, K. Takahashi, I. Honda, M. Matsushima, Bull. Chem. Soc. Jpn. 64 (1991) 2508; 65 (1992) 1240.
[44] H. Sato, K. Hirose, N. Ishii, H. Tojima, M. Kitamura, Jpn. Patent Sho 62-281856, 1987, Sumitomo Chemical.
[45] H. Sato, K. Hirose, M. Kitamura, S. Nakamura, Proceedings of the Eighth International Zeolite Conference, 1989, p. 1213.
[46] M. Niwa, S. Morimoto, M. Kato, T. Hattori, Y. Murakami, Proceedings of the Eighth International Congress on Catalysis, Berlin, 1984, vol. IV, p. 701.
[47] W.F. Hoelderich, M.E. Paczkowski, Stud. Surf. Sci. Catal. 83 (1994) 399.

[48] K. Inumaru, T. Okuhara, M. Misono, Chem. Lett. (1992) 1995.
[49] H. Fukui, Hyomen (Surface), (1994) 131.
[50] N. Kodakari, N. Katada, M. Niwa, J. Chem. Soc., Chem. Commun. 623 (1995).
[51] T. Ito, H. Kanai, T. Nakai, S. Imamura, React. Kinet. Catal. Lett. 52 (1994) 421.
[52] C. Dossi, R. Psaro, A. Bartsch, A. Fusi, L. Sordelli, R. Ugo, M. Bellatreccia, R. Zanoni, G. vlaic, J. Catal. 145 (1994) 377.
[53] C. Dossi, R. Psaro, A. Bartsch, E. Brivo, A. Galasco, P. Losi, Catal. Today 17 (1993) 527.
[54] B.S. Kwak, W.M.H. Sachtler, J. Catal. 145 (1994) 456.
[55] Y. Okamoto, T. Imanaka, K. Asakura, Y. Iwasawa, J. Phys. Chem. 95 (1991) 3700.
[56] Y. Okamoto, A. Maezawa, H. Kane, I. Mitsushima, T. Imanaka, J. Chem. Soc., Faraday Trans. I 84 (1988) 851.
[57] A. Brenner, R.L. Murwell Jr., J. Am. Chem. Soc. 97 (1975) 2565.
[58] C. Dossi, R. Psat, R. Ugo, Z.C. Shang, W.M.H. Sachtler, J. Catal. 149 (1994) 92.
[59] C. Dossi, R. Psato, A. Bartsch, A. Galasco, E. Brivio, P. Losi, Catal. Today 17 (1993) 527.
[60] K. Asakura, K. Aoki, Y. Iwasawa, J. Mol. Catal. 74 (1992) 345.
[61] G.C. Bond, K. Bruckman, Faraday Discuss., Chem. Soc. 72 (1981) 235.
[62] G.C. Bond, P. Konig, J. Catal. 82 (1982) 309.
[63] T. Hattori, M. Matsuda, K. Suzuki, A. Miyamoto, Y. Murakami, Proceedings of the Ninth International Congress on Catalysis, Calgary, 1988, p. 1640.
[64] T. Hattori, S. Ito, T. Tagawa, Y. Murakami, in: B. Delmon, P. Grange, P.A. Jacobs, G. Poncelet (Eds.), Preparation of Catalysts IV, 1987, p. 113.
[65] J.S. Yoo, J.A. Donohue, M.S. Kleefisch, Appl. Catal. A 110 (1994) 75.
[66] J.S. Yoo, P.S. Lin, S.D. Elfline, Appl. Catal. A. 106 (1993) 259.
[67] J.S. Yoo, Appl. Catal. A 142 (1996) 19.
[68] J.S. Yoo, P.S. Lin, S.D. Elfline, Appl. Catal. A 124 (1995) 139.
[69] J.S. Yoo, Appl. Catal. A 135 (1996) 261.
[70] M. Aresta, C. Fragele, E. Quaranta, I. Tommasi, Chem. Soc., Chem. Commun. (1992) 315.
[71] J.S. Yoo, Appl. Catal. A 143 (1996) 29.
[72] J.S. Yoo, C. Choi-Feng, J.A. Donohue, Appl. Catal. A 118 (1994) 87.
[73] J.S. Yoo, C. Choi-Feng, in: J.W. Hightower, W.N. Delgass, E. Iglesia, A.T. Bell (Eds.), Proceedings of the 11th International Congress – 40th Anniversary Stud. Surf. Sci. Catal., vol. 101, Elsevier, Amsterdam, 1996, p. 1021.
[74] J.S. Yoo, A.R. Sohail, S.S. Grimmr, C. Choi-Feng, Catal. Lett. 29 (1994) 299.
[75] J.S. Yoo, A.R. Sohail, S.S. Grimmer, J.Z. Shyu, Appl. Catal. 117 (1994) 1.
[76] M. Schbeider, A. Baiker, Catal. Rev. Sci. Eng. 37(4) (1995) 515.
[77] B. Na, Y. Lee, Chokmae (Catalysis, Korea) 12(2) (1996) 18.
[78] S. Niwa, F. Mizukami, M. Toba, R. Kutsuzawa, Shokubai 37(2) (1995) 140.
[79] S.R. Mirzabekova, A.Kh. Mamedov, M.I. Rustamov, Kinet. Catal. 36(1) (1995) 121.